coatings

MDPI

Article

Evolution of Elements on Electrode Surfaces in Gas-Insulated Systems under Electrical Heating

Jixing Sun [1,*], Kun Zhang [1], Kaixuan Hu [1], Jiyong Liu [1,2], Yu Tian [3], Xin Wang [2] and Shengchun Yan [4]

[1] School of Electrical Engineering, Beijing Jiaotong University, Haidian District, Beijing 100044, China
[2] Shuohuang Railway Development Co., Ltd. of National Energy, Cangzhou 062350, China
[3] China Electric Power Research Institute Co., Ltd., Haidian District, Beijing 100192, China
[4] National Energy Transportation Technology Research Institute Co., Ltd., Beijing 100080, China
* Correspondence: jxsun@bjtu.edu.cn or sanyou345@163.com; Tel.: +86-158-0106-7328

Abstract: Accidents always occur in gas-insulated switchgears (GIS) and gas-insulated lines (GIL) since filmed joint electrodes are produced when internal gases react with the electrode's surface when there is a discharge or when internal electricals overheat. To solve the problem, this paper analyzed the evolution of elements on the contact electrode. The reaction of the SF6 and electrode's surface under breakdown currents and overheating conditions was obtained, and the discharge time and discharge current effects upon the transfer of the element were proposed. It was found that the mobility of the F element on the electrode's surface typically increases after electrical heating. The number of interruptions and short-circuit currents are important factors affecting the transfer of the F element to the electrode. The flashover current is the essential factor that accelerates the transfer of the F element to insulating materials. Frequent switching is a main factor that accelerates the transfer of the F element to the contact. It was also found that Al has little correlations with the breaking process, and metal fluorides become the main components on the electrode's surface under discharge heating. The research provides a theoretical basis and data support for GIS/GIL surface optimization treatments and the improvement of fault detection methods.

Keywords: UHV; gas insulation; SF_6; electrode; decomposition product; surface treatment

Citation: Sun, J.; Zhang, K.; Hu, K.; Liu, J.; Tian, Y.; Wang, X.; Yan, S. Evolution of Elements on Electrode Surfaces in Gas-Insulated Systems under Electrical Heating. *Coatings* **2023**, *13*, 33. https://doi.org/10.3390/coatings13010033

Academic Editor: Alessandro Latini

Received: 26 November 2022
Revised: 19 December 2022
Accepted: 21 December 2022
Published: 25 December 2022

1. Introduction

When the gas-insulated switchgear (GIS) operates frequently or has defects, the SF_6 gas will decompose, react with electrodes and other solid insulating materials, and form solid decomposition products. These solid deposits are generated on the surface of the electrodes and the walls of the equipment's shell. Composition analyses can reveal the evolution and migration of elements inside the equipment under electrical heating conditions and provide a basis for the evaluation of equipment operation statuses.

For the detection of GIS faults and insulation conditions, reference [1] proposes 23 comprehensive evaluation index systems that comprehensively considered partial discharge (PD) hazards, SF_6 insulation performance, time, environment, and economy and established an evaluation model for GIS equipment insulation conditions. The model solves the problems of setting the weight of the evaluation index and determining the membership, and the experimental example shows that the evaluation results are reasonable. Reference [2] studies some important factors that affect the surface flashover characteristics of solid insulators in SF_6. The reliability of gas-insulated equipment can be well maintained via preventive measures and management. Reference [3] studied the influence of common failure modes (such as corrosion, disconnection, and contact misalignment) on the dynamic resistance measurements (DRM) using COMSOL finite element analysis. A three-dimensional multi-physics simulation of the breaking chamber is carried out, and it is proposed that DRM exhibits specific behaviors in each specific fault, and the performance of the algorithm is evaluated in experiments. Reference [4] proposes a method for detecting

PD in GIS epoxy insulators using a new characteristic gas named carbonyl sulfide (COS) and experimentally confirms that COS occurs only when the partial discharge intensity is sufficient for causing flashovers in epoxy insulators. The relationship between the discharge power and the COS concentration growth law obtained from the experiment is proposed, which can be used to diagnose the high-energy discharge epoxy solid insulation in GIS. Reference [5] introduced a gas detection system based on the PA effect and studied the photoacoustic spectrum and temperature characteristics of SF_6 decomposition components under partial discharge. A temperature linear correction model is proposed, which lays a foundation for the development of an online monitoring device for SF_6 decompositions.

Regarding the decomposition the by-products of SF_6 in various discharge modes and its related influencing factors, reference [6] uses ESCA, SEM, FTIR, and thermal analysis methods to analyze the structure and morphology of seven commercial epoxy-insulating fluids in arcing by-products and low-energy flashover sparks. It was found that for the voltage tracking performance and the corrosion resistance of SF_6 arc by-products, filling materials and resins are key factors, and no single material was found to have the most ideal effect. Reference [7] summarizes the qualitative and quantitative results of SF_6 by-products and their formation rates under various discharge modes. It was proposed that the electron, ion, and neutral reaction rates in SF_6 discharge need to be further analyzed based on phenomenological observation to better understand the decomposition mechanism and the impact of products on equipment. Reference [8] proposes using the applied voltage and SF_6 pressure to describe the electric field strength and gas density, respectively; a 50 Hz AC discharge experiment was carried out, under different applied voltages and different SF_6 pressures using point-to-plane electrodes. The influence of the applied voltage and SF_6 pressure was analyzed, and the experimental equation describing the relationship between the change in the SF_6 gas by-product and SF_6 pressure was derived. Reference [9] found the characteristics of SF_6 decompositions under PD by comparing the decomposition data of SF_6 under different voltages. The ratio reaches a steady state after 72 h, and $c(CF_2 + CS_2)/c(CO_2)$ and $c(SO_2)/c(SO_2F_2)$ can be used as the fault severity characteristic ratio of free metal particle defects. Reference [10] studied the decomposition products of SF_6 under three superheating conditions: solid insulation overheating, metal overheating, and metal adjacent to the insulating material overheating. The types of overheating can be identified based on the characteristic ratio of $(SOF_2 + SO_2)/(CO + CO_2)$ and the characteristic products of SF_6 decomposition. Reference [11] studies the decomposition characteristics of SF_6 under a negative partial discharge (PD) in different cases, and they found that the decomposition characteristics of SF_6 are closely related to the PD status. They used a fuzzy comprehensive evaluation to establish a local discharge fault state evaluation model, which lays a foundation for the comprehensive evaluation and fault diagnosis of the DC GIE insulation state in future. Reference [12] uses the density functional theory (DFT) to analyze the micro-water decomposition process of CF_3I under ambient temperature and pressure, and they observed that H_2O will destroy the insulating properties of CF_3I. Reference [13] studied typical defects (metal protrusions and metal particles) of the decomposition characteristics of SF_6 decomposition products, and the authors proposed that under the same discharge intensity, the difference in CO_2 generation rates is small with respect to these two defects. In addition, the sulfide generation rate under protruding metal defects was higher than that under metal particle defects. Reference [14] designed a gas chamber and four typical artificial defects to simulate the decomposition of SF_6 under GIS partial discharges, and the concentrations of decomposition products under the four defects were determined by gas chromatography. They observed that it was feasible to identify the type of PD by using an analysis of SF_6 decomposition products. Reference [15] selected the concentration and concentration ratio of SF_6 decomposition products as characteristic quantities based on the data of SF_6 decomposition products under four PDs, uses a fuzzy c-means clustering algorithm to evaluate the performance of these two types of feature quantities. It was found that in PD identification, the performance based on the concentration ratio as a characteristic quantity is better than that based on the concentration. Reference [16]

constructed an experimental test system, studied the characteristics of SF_6 decomposition components in the presence of trace moisture, and analyzed the SF_6 decomposition product. The influence of moisture contents on the decomposition products was discussed compared with normal operations, and the gas decomposition mechanism involving moisture was discussed. Reference [17] conducted a series of artificial thermal failure decomposition experiments with different water concentrations on the self-designed SF_6 thermal decomposition experimental system and proved that water plays an important role in the generation of SF_6 thermal decomposition components. Reference [18] analyzed the SF_6 decomposition products in different equipment and pointed out the characteristic gases of the fault characteristics of the gas insulation equipment and their application prospects. Reference [19] proposed the further research topic of SF_6 decomposition in combination with the requirements of GIS equipment status assessments. They obtained the criterion of SF_6 decomposition products in GIS fault diagnosis and provided the basis for GIS operation management. Reference [20] used quadrupole mass spectrometry to study the formation of spark discharge decomposition by-products in SF_6, quantified the amount of spark discharge by-products in SF_6, and determined the energy and pressure dependence of various by-products. References [21,22] proposed the advancement of photo- and electrocatalytic nanomaterials via pulsed laser-assisted technologies with detailed mechanistic insights and structural optimization along with effective catalytic performances in various energy and environmental remediation processes. Moreover, in reference [23], in order to study the potential antibacterial properties of the materials, two different bacterial strains were used, and the diameter of the zone of inhibition was observed. However, there is no other public report on the evolution characteristics of elements inside the switchgear and on the surface of the electrode under discharge heating.

In this paper, the reaction process of SF_6 gas with the electrode's surface and insulating material under the superheated conditions of GIS/GIL is carried out, and the micro-morphological characteristics and element distribution of the material's surface are obtained; moreover, an accurate observation method for the surface's morphology is proposed. The influence characteristics of discharge current on the transfer of the F element provide the theoretical basis and data support for GIS/GIL failure analysis, surface treatments, and electrode optimization.

2. Elemental Reaction Process on the Electrode's Surface under Electrical Heating Conditions

Due to the operation of circuit breakers, isolating switches, and earthing switches, high temperature arcs and mechanical wear may produce solid powders. At the same time, when switchgear (including GIS busbars, transformers, etc.) has discharges or overheating defects, solid decomposition products may also be produced [24].

For circuit breakers, under the high temperature conditions of the breaking arc, SF_6 gas and insulating materials (CkHy) such as graphite (C), polytetrafluoroethylene (Teflon or PTEE), contact material (Cu and W), arc-extinguishing structural materials, shell materials (Al), etc., will produce chemical reactions [25], and they mainly include the following.

$$SF_6 + Cu \rightarrow SF_4 + CuF_2 \quad (1)$$

$$2SF_6 + W + Cu \rightarrow 2SF_2 + WF_6 + CuF_2 \quad (2)$$

$$3SF_6 + W \rightarrow 3SF_4 + WF_6 \quad (3)$$

$$4SF_6 + W + Cu \rightarrow 4SF_4 + WF_6 + CuF_2 \quad (4)$$

$$4SF_6 + 3W + Cu \rightarrow 2S_2F_2 + 3WF_6 + CuF_2 \quad (5)$$

$$Al + 3F \rightarrow AlF_3 \quad (6)$$

$$2CF_2 + SF_6 \rightarrow 2CF_4 + SF_2 \quad (7)$$

In the above reactants, some products such as WF_6, AlF_3, CuF_2, etc., all exist in the switch arc's extinguishing chamber as steady-state solid powders.

2.1. Discharge Defects

When a discharge defect occurs inside the equipment, SF_6 gases interact with solid materials, and polymer materials and metal materials are decomposed by high-temperature arcs, releasing metal vapor and cracking products such as methane, CO_2, etc. [26]. SF_6 gases and their decomposition products, such as the gas-phase reaction [27], are accompanied by the volatile substances produced during the arc-extinguishing process, as shown in Equations. (8) and (9). These decomposition products react with metallic materials, silicon-insulating basin materials, etc., to produce solid and powdered metal fluorides.

$$SF_6 \rightarrow SF_4 + 2F \rightarrow SF_2 + 4F \tag{8}$$

$$M + xF \rightarrow MF_x \tag{9}$$

Among them, M represents metals or the C element. Since polymer materials can absorb water, volatile substances contain a large number of water molecules and affect gas-phase reactions. Initially, SF_4 reacts with moisture to form SOF_2, and then it will react with water on the surface of the insulator for a long period of time, resulting in the slow generation of SOF_2 within a few hours of discharge. The reaction formula is as follows.

$$SF_4 + H_2O \rightarrow SOF_2 + 2HF \tag{10}$$

$$SOF_2 + H_2O \rightarrow SO_2 + 2HF \tag{11}$$

Due to the rapid response of formula (10), SF_4 can be detected rarely. When the HF molecule encounters the silicon filler, a chemical reaction can occur according to Formula (12) to generate SiF_4 gas. Equation (13) reacts rapidly when silica is present in the form of quartz, and the pressure build-up leads to the formation of bubbles.

$$SiO_2 + 4HF \rightarrow SiF_4 + 2H_2O \tag{12}$$

$$SiF_4 + 2HF + H_2O \rightarrow H_2SiF_6 + H_2O \tag{13}$$

In Equation (13), the generated water bubbles contain highly electrolytic materials such as H_2SiF_6, and the HF gas absorbed by the epoxy resin changes the surface resistance, which may lead to a significant drop in the shock flashover voltage. For the mixtures of SF_6 and perfluorocarbons, the C atoms in the perfluorocarbons react with the F atoms of the SF_6 gas to form inert perfluorocarbon compounds [28]. The nozzle's wear is manifested as the "burning" of Teflon, and reaction formula (14) occurs, resulting in the reaction of PTFE and SF_6 to generate CF_4, carbon fluoride, SF_4, etc.

$$(\text{-}CF_2\text{-})_n + SF_6 \rightarrow (\text{-}CF_2\text{-})_{n-1} + CF_4 + SF_4 \tag{14}$$

Solid insulating materials in switchgear are often made of polymer materials such as epoxy, polyethylene, Teflon, and phenolic, including filled epoxy materials for GIS basin insulators [29]. A flashover occurs at the interface of SF_6 gases and solids (insulating basin creepage flashover), and the polymer material in the discharge will affect the formed decomposition products. The test results show that when the main product generated by the arc is CF_4, the gas products generated by the thermal performance degradation of epoxy and phenolic resins will cause a large amount of solid decomposition products.

2.2. Overheating Defect

The thermal and chemical stability of SF_6 gas at the normal operating temperature of GIS is an important characteristic, which has a great influence on the long-term reliability and aging performance of the equipment [30]. Compared with the discharge decomposition

products, the decomposition process's products under overheating defects have not been fully studied.

Experiments show that [31] the critical temperature of SF_6 gas decompositions is 600 K, which is mainly decomposed into SF_2 and SF_4. At 150 K, SF_6 gases will react with silicon steel sheets. When the temperature is higher than 200 K, many metals begin to react with SF_6 to form metal fluorides and sulfide. In addition to the formation of fluoride and sulfide on the surface of the metal casing, gaseous decomposition products such as SO_2 can also be detected.

The decomposition rate of SF_6 increases significantly with increasing temperatures [32]. At 650 K, when aluminum and copper are placed in SF_6 gas for 90 h, SOF_2, SO_2F_2, and SO_2 will be generated, and stainless steel has no decomposition products. For aluminum, only SO_2F_2 is detected. For copper, SO_2 and SOF_2 are detected, and a large amount of SO_2 is detected in the test. Metal fluorides simultaneously formed [33].

When the temperature is between 700 to 900 K, SF_6 gas in stainless steel, copper, and quartz tubes decomposes into SF_4. For quartz tubes, SF_4 reacts with SiO_2 to form SiF_4 and SOF_2. For copper and stainless-steel tubes, SF_4 is the main decomposition product. When the temperature reaches 1500 K, SF_6 mainly decomposed into SF_4, and its conversion to oxyfluoride depends on SF_6 gas and impurities contained on the metal's surface, such as oxygen and moisture. SF_6 gas decomposition products react with metals and insulating materials to form solid powders such as metal fluorides and fluorocarbons.

3. Experimental Detail and Sample Preparation

3.1. Experimental Detail

The opening and closing tests were conducted in the high-power test station (50MVA, Shandong Taikai High Voltage Switchgear Co., Ltd, Taian, China) with a high electrical life capacitor bank circuit breaker. The main diagram of the test circuit is shown in Figure 1.

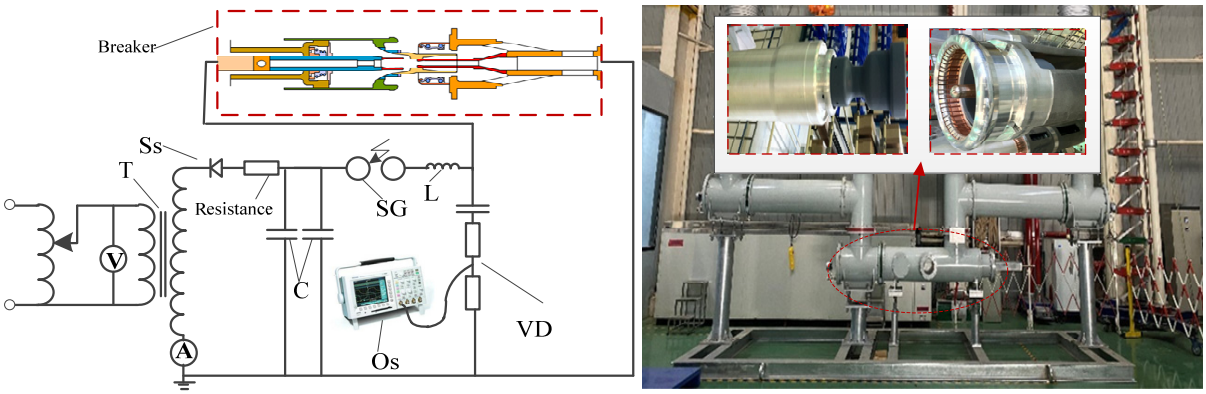

Figure 1. Circuit diagram of circuit breaker on load breaking and making tests. C—Impact capacitor; SG—steepen ball; R—tuning resistance; L—tunable inductor; VD—resistance voltage divider; CRO—oscilloscope.

The static contact structure part in the arc's extinguishing chamber is supported and fixed by the insulator, and the static contact structure mainly comprises a static contact base, a static main contact, a static arc contact, and other structures. The overall voltage withstanding the capability of the circuit breaker is improved by increasing the insulation distance between the main conductor circuit part of the circuit breaker and the casing of the test device. The moving contact is mainly composed of a moving contact seat, a moving main contact, a moving arc contact, a cylinder, and a tie rod. The moving contact is connected with the insulating pull rod outside the tank body, and the opening and closing movement of the circuit breaker contact is driven by the transmission device connected with the contact. Since the discharge or high-temperature arc between the arc contacts during the test will ablate the contacts, the dynamic and static arc contacts are made of

copper–tungsten alloy materials in order to improve the burning resistance of the arc contacts of the circuit breaker and to meet the requirements for multiple tests at different spacings [34–37].

3.2. Main Equipment for Sample Preparation

After the test was completed, the surface of the electrode was observed by using scanning electron microscopes (COXEM, Daejeon, Korea), and the elements on the surface of the electrode were analyzed. The equipment and main parameters used are shown in Table 1.

Table 1. Main parameters of the equipment.

No	SEM Composition	Performance Parameters	Technical Indicators
1	SEM	Resolution	Secondary electron image: 3 nm (30 kV), 8 nm (3 kV), 15 nm (1 kV), Backscattered electron image: 4 nm (30 kV).
2		The accelerating voltage	0.5 kV∼30 kV continuously adjustable
3		Magnification	5∼300,000 times, adjustable

3.3. Sample Preparation

An SEM analysis was carried out to obtain the characteristics of non-metallic adhesion on the electrode's surface [38]. The result shows that the solid decomposition products collected inside the switchgear were mainly powder particles. The sample preparation method includes the direct dusting method, dispersant dispersion method, ultrasonic dispersion method, etc. For powder samples with different particle sizes, it is necessary to select an appropriate method to achieve the best observation effect. According to the requirements of SEM testing samples, the samples were prepared by using the direct dusting method, dispersant dispersion method, and ultrasonic method. The processing steps of solid samples were analyzed, and the sample preparation process of the solid decomposition products was proposed, as shown in Figure 2. It mainly includes (1) sampling, (2) physical cleaning to remove dirt and impurities on the surface of the sample, (3) drying treatments in which the cleaned sample should also be dried by using an appropriate method; (4) and fixing (using conductive tape to fix the pre-processed sample on the sample stage). (5) Then, the sample with poor electrical conductivity needs to be sprayed with gold to coat the conductive film. The selection of gold spraying times and gold spraying currents should be determined according to the properties of the sample. Usually, the gold spraying time should not be too long, and the spraying current should not be too large in order to prevent damage with respect to the sample or change the shape of the sample.

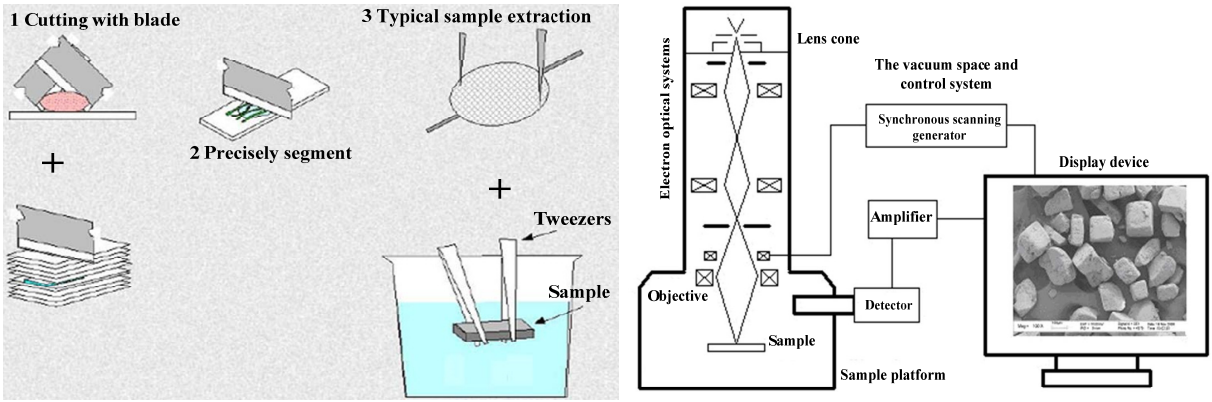

Figure 2. Sample preparation process and schematic diagram of the main components of the SEM.

4. Evolution Characteristics of Electrode Surface Elements during the Experiment

4.1. Sample Test Results in the Test Switch

The high electrical life capacitor bank circuit breaker used in UHV engineering was subjected to breaking and closing tests at the high-power test station. After more than 1300 tests, the circuit breaker failed to break. In order to analyze the reasons for the failure of the circuit breaker test, gas was collected from the equipment to analyze the composition of SF_6 gas decomposition products.

The output spectrum obtained by a pulsed discharge detector (PDD) is shown in Figure 3. The main components detected are CF_4, C_2F_6, and C_3F_8. The content of each component is analyzed and there are high levels of carbide content, indicating the reaction generated between the SF_6 and the insulator in the GIS.

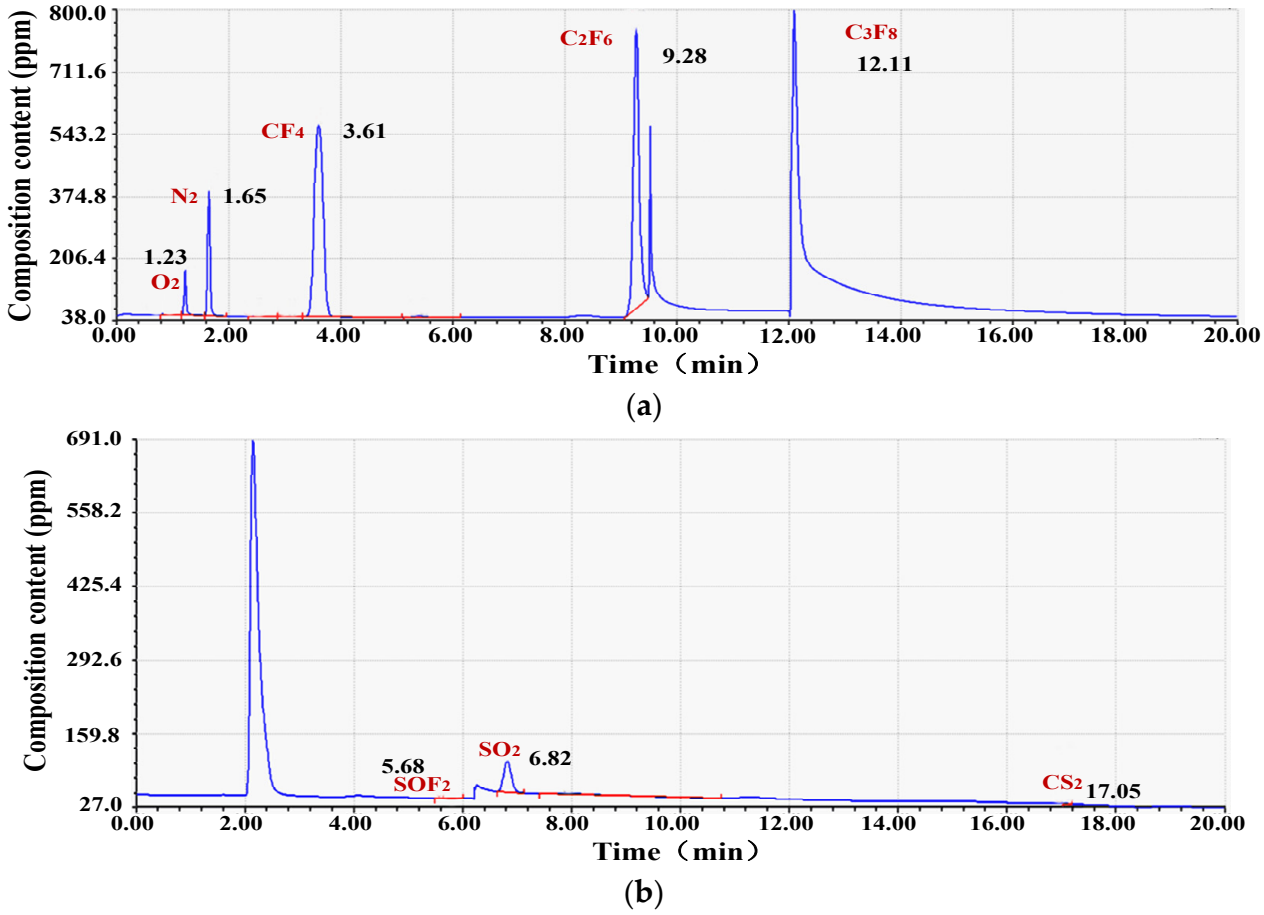

Figure 3. Test results of gas in the test switch. (**a**) PDD1 chromatogram. (**b**) PDD2 chromatogram.

Since the circuit breaker completed more than 1300 breaking tests and the breaking tests failed, the gas's composition is analyzed in Table 2, and a large number of powdery solid decomposition products were deposited in the arc-extinguishing chamber. The solid decomposition products were collected from the arc-extinguishing chamber for detection and analysis with an electron microscope. The tungsten filament scanning electron microscope in the laboratory was used to observe appearances and morphologies, and the results are shown in Figure 4. At the same time, the samples were detected and analyzed with a field emission electron microscope.

The typical element composition upon arcing contact is shown in Figure 4b at a single test point.

Table 2. Gas composition of test circuit breaker samples.

No.	Gas		Content (μL/L)
1	Carbide	CO	7.3
2		CF_4	816.96
3		CO_2	22.63
4		C_2F_6	2416.27
5	Sulfide	SOF_2	1.47
6		SO_2	33.33
7		CS_2	51.27

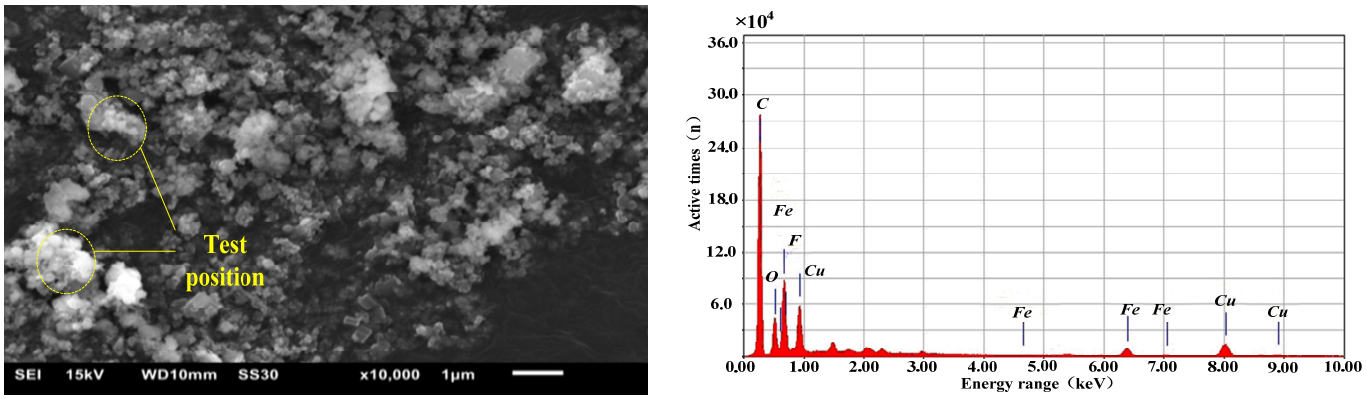

Figure 4. Morphological observation and composition analysis of solid powder in the test circuit breaker. (**a**) Appearance. (**b**) Component.

Results comparing and analyzing the elemental composition at multiple analysis points are listed in Table 3. Because the contact that the circuit breaker makes participates in the reaction, Cu is detected as the main component, indicating that the proposed detection method is feasible.

Table 3. Comparison of sample test results of test circuit breakers. (a) Content detected by field emission electron microscope (%).

Elemental Composition	C	O	F	Al	S
Content (%)	16.62	8.72	41.83	4.52	0.53
Elemental Composition	**CR**	**Cu**	**Ag**	**W**	-
Content (%)	0.86	24.53	1.69	0.70	-

The field-emission electron microscope test method was used to detect the F, Al, and Cu, with different breaking tests until the electrode's surface is ablated. After being normalized, the three elements changing with operation times is shown in Figure 5. Element F increases and Cu decreases, and Al exhibits a slight increase. This indicates that Equation (1)'s reaction is persistent and obvious; after all, the arc was generated on the electrode's surface.

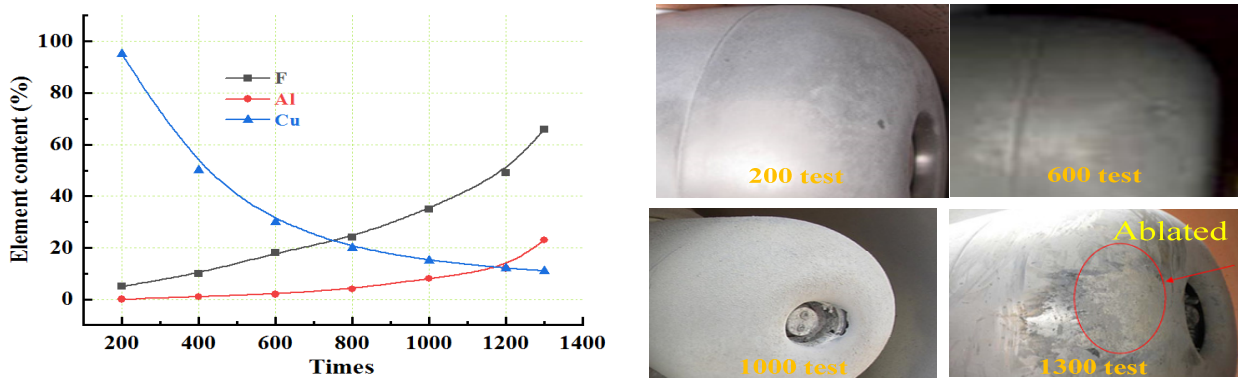

Figure 5. The element on test electrode's surface. (**a**) is element changing of electrode surface with breaking tests (**b**) is surface morphology of the electrode.

4.2. Element Transfer Test and Case Analysis under Electrical Heating Conditions

For the 550 kV gas-insulated circuit breaker, 20 electrical life tests with 100% rated short-circuit breaking current was conducted. The SF_6 gas state data detected by a portable gas chromatograph and a detection tube are listed in Table 4. It can be seen that the decomposition contents in the equipment are all high, and CF_4 and SO_2 contents reached thousands to tens of thousands of uL/L.

Table 4. SF_6 gas state detected in a 500 kV circuit breaker.

Purity (%)	Decomposition Product Composition			
	Air (μL/L)	CF_4 (μL/L)	SO_2 (μL/L)	HF (μL/L)
99.3	3478	5066	11,550	10,000

In order to analyze the influence of the number of short-circuits on the element transfer process, a comparative test was carried out with short circuit current 34.8 kA. The detection results of SF_6 gas decomposition products are shown in Table 5. A small amount of SO_2 and HF gas is detected and the arc discharge produces a large amount of SF_6 gas decomposition product components SO_2 and HF gas.

Table 5. Composition of SF_6 gas in the circuit breaker during comparative tests.

	Phase	SO_2(μL/L)	HF(μL/L)
SF_6 circuit breaker	A	5	12
	B	1800	90
	C	1800	120

Faulty switch equipment

(1) Combined with research, the in-service 550 kV circuit breaker is analyzed. After the circuit breaker is overhauled, there is a short circuit on the line where it is located, and the circuit breaker is disassembled, as shown in Figure 6.

The electrode's surface material was collected, and the SF_6 gas decomposition products were detected. The results are shown in Table 6. The high content of SO_2 gases indicates that a serious arc discharge fault occurred inside the equipment.

Figure 6. Contact photos of the test circuit breaker.

Table 6. Test results of SF_6 gas composition of the 550 kV circuit breaker.

Composition	CF_4	SO_2	H_2S
Content (μL/L)	4264	>5000	>1600

(2) Another line where the 550 kV circuit breaker is located at exhibits differential protection, and the circuit breaker has an insulation discharge fault. The detection results of SF_6 gas decomposition products are listed in Table 7, indicating that the content of SO_2 gas components seriously exceeds the standard. The fault circuit breaker was disassembled and inspected, and it was found that there was a breakdown between the pressure-equalizing cover and the outer shell, and the discharge trace was located in the lower part of the tank. There are obvious arc discharge traces on the voltage-equalizing cover at the end of the resistor.

Table 7. Test results of SF_6 gas composition of 550 kV circuit breaker.

Composition	SO_2	H_2S	HF
Content (μL/L)	>1500	>200	>900

The solid sample was analyzed by scanning electron microscope and energy dispersive spectrometer. The analysis report is shown in Figure 7. The main elements detected are the F content of 49.15% and the Al content of 32.32%. It can be seen that the solid sample comprises mainly metal fluoride.

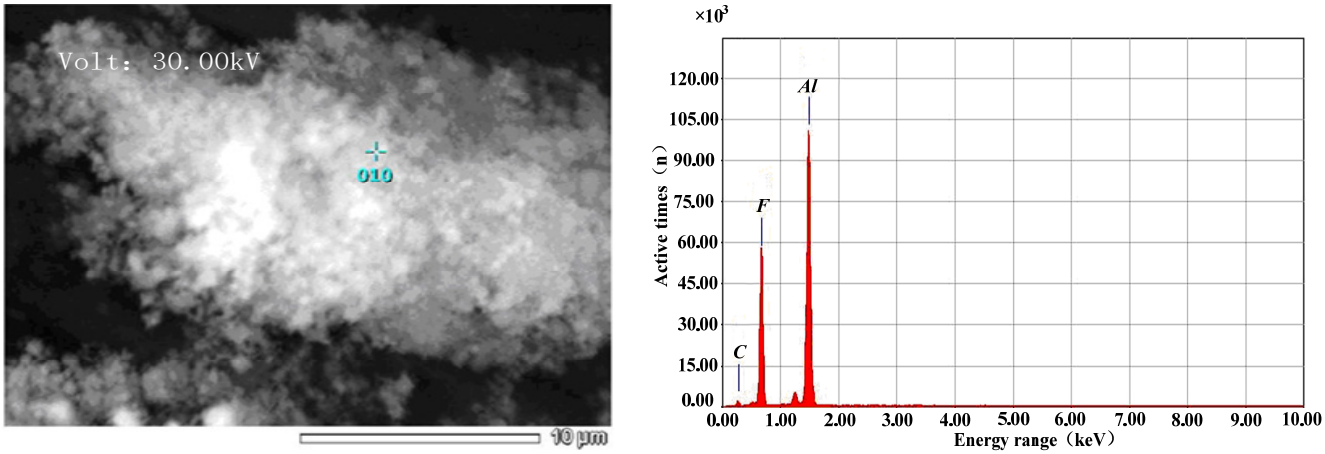

(**a**) (**b**)

Figure 7. Inspection GIS solid samples with a scanning electron microscope and energy spectrum. (**a**) Microscopic morphology of surface material. (**b**) Element distribution.

Due to the discharge of the GIS busbar, the main metal materials of the high-voltage guide rod and the casing comprise aluminum and aluminum fluoride. It can be seen

that the combination of using the scanning electron microscope and energy spectrometer can determine the elemental composition and relative content of the solid sample and determine the element transfer process on the surface of the SF_6 environmental contact under the action of electric heat.

(3) Running switchgears

As a comparison, the solid powder on the electrode surface of the 500 kV GIS equipment in stable operation was analyzed, and the relationship between the element composition of the solid decomposition products and the equipment status or failure was counted. The SO_2 gas content detected in the equipment gas chamber was all less than 1 uL/L. At the same time, the solid powder deposited in the arc-extinguishing chamber of the circuit breaker was collected, tested, and analyzed in lab, and they are sorted into Table 8 (1#–4#).

Table 8. Detection results of solid decomposition products in different circuit breakers.

Equipment Conditions			Elemental Composition Content (%)								
			F	**Al**	**Cu**	**W**	**Fe**	**C**	**S**	**O**	**Si**
Running Breaker	1#		2.53	13.14	3.42	1.05	23.01	/	1.22	/	11.44
	2#		/	17.83	/	/	1.14	0.68	0.58	44.66	22.75
	3#		/	15.07	/	/	2.21	/	0.17	41.37	28.04
	4#		/	19.87	/	/	0.49	/	0.45	43.51	23.9
Faulty 550 kV circuit breaker	5#	1 [a]	58.24	24	16.46	/	0.3	/	/	/	0.41
		2 [b]	57.15	23.82	15.15	0.12	0.3	/	0.31	/	0.37
	4#	1 [a]	66.44	16.74	/	/	2.68	14.13	/	/	/
		2 [b]	62.21	13.89	/	/	3.53	20.36	/	/	/
Test circuit breaker	7#		63.54	19.24	8.45	1.05	2.94	3.95	0.67	/	/
	8#		17.04	1.22	31.06	18.59	2.25	/	1.17	21.84	5.98

Note: [a] is the first test; [b] is the second test.

(4) Analysis of test results

The solid powder samples collected from circuit breakers under different working conditions were compared and analyzed, and the elements contained in the detected solid samples were counted, mainly including F, Al, Cu, W, Fe, C, S, O, Si, etc. The detection results of the solid decomposition products of the above three types of equipment (eight circuit breakers) are listed in Table 8. F, Al, and Cu are the main elements, and the percentage of each element is shown in Figure 8. Corresponding to the equipment's working conditions, 1−4 in the figure are normal operation circuit breakers, 5−8 are fault circuit breakers, and 9−10 are test circuit breakers. It shows that the solid powder in the circuit breaker comprises mainly metal fluoride.

An analysis of the content of the main element components F, Al, and Cu in Table 8 shows that the content ratio of F, Al, and Cu in the solid powder in the switchgear varies with different equipment operating conditions and fault types.

(1) For equipment in normal operation, the detected element F content is low; Cu, W and C are detected less; Fe and S contents are low; Al, O, and Si contents are slightly higher.

(2) The switchgear was tested, and the arc discharge breaking test was carried out. The discharge energy was relatively large, which may involve the metal material in the contact and the insulating material inside the arc-extinguishing chamber. Large contents of elements F, Al, Cu, W, were detected and C, O, S and Si were less detected.

(3) After the failure of the equipment, a large amount of elements F and Al were detected. An arc discharge fault occurred inside the circuit breaker of the Jiangling converter station, involving copper or copper alloy materials in the contacts, and a high content of the element Cu was detected. The fault circuit breaker of Huojia substation is an internal insulation fault, the discharge energy is slightly smaller, and the detected elements Cu and W content are small, which may involve insulating materials, and element C is detected.

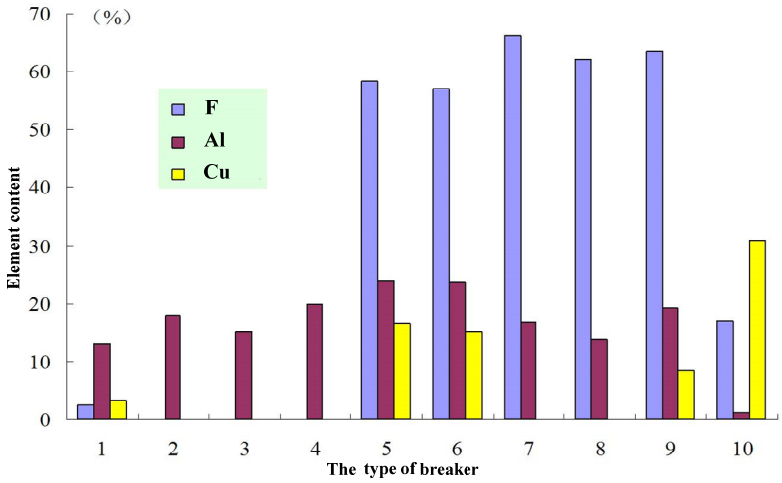

Figure 8. Elemental content analysis of solid powder in switchgear.

The above analysis shows that the F element in the gas-insulated equipment will gradually evolve into the metal to form metal fluorides; the F content of the normal operation equipment is low; the F content of the solid powder during multiple interruptions or in the fault circuit breaker is high. The Cu element is related to whether the circuit breaker is broken or not. A large amount of Cu content was detected in the solid powder when arc discharges occur during breaking, and the contacts are ablated. The Al element's content has little correlation with the breaking process, which characterizes the aluminum parts in the arc-extinguishing chamber, and elemental Al was detected in all circuit breakers due to long-term slow reactions with SF_6 gases or from adsorbents. Therefore, by detecting the content of F, Al, and Cu in the solid powder in the switchgear, it is possible to judge the operation status of the device and the type and degree of failure.

5. Conclusions

In this paper, based on GIS/GIL, the reaction process of SF_6 gas with the electrode's surface and insulating material was analyzed under superheated conditions, and the micro-morphological characteristics and the element distribution of the material surface were obtained. By comparing the experimental and test results, the conclusions are as follows.

(1) Samples collected from the switch and field equipment were tested using the SEM method. The results show that after discharge heating, gas components such as CF_4, CS_2, and SO_2 increase in the gas's composition, indicating that the SF6 gas reacted with the insulator in the GIS.

(2) Comparing the breaking times, short-circuit currents, and element transfer processes under flashover fault conditions, it was found that the increase in breaking times and short-circuit current is an important factor affecting the conversion of F elements to the electrode, and the flashover current is the key factor for accelerating the transfer of F elements to the insulating material.

(3) Frequent breaking is the main factor for accelerating the transfer of F elements to the contact. The content of element Al has little correlation with the breaking process. This observation indicates that the long-term slow reaction between the aluminum parts in the arc-extinguishing chamber, the SF_6 gas or the effect of the adsorbent, and the type and degree of GIS failures can be identified by detecting F, Al, and Cu in solid powder in switchgear.

Author Contributions: Conceptualization, J.S. and K.Z.; Methodology, Y.T.; Software, X.W.; Validation, S.Y.; Formal analysis, K.H.; Investigation, J.L.; Resources, X.W.; Data curation, K.H.; Writing—original draft, J.S. and S.Y.; Writing—review & editing, J.S. and K.Z.; Visualization, X.W.; Supervision, S.Y.; Project administration, Y.T.; Funding acquisition, J.S., K.Z. and J.L. All authors have read and agreed to the published version of the manuscript.

Funding: This work was supported by the Fundamental Research Funds for the Central Universities (Science and technology leading talent team project, 2022JBQY008), National Natural Science Foundation of China (51907003) and Technology Project of National Energy Group (SHTL-21-08).

Institutional Review Board Statement: Not applicable.

Informed Consent Statement: Not applicable.

Data Availability Statement: The authors confirm that the data supporting the findings of this study are available within the article.

Acknowledgments: The authors would like to thank reviewers for their pertinent comments that helped improve the quality of this paper.

Conflicts of Interest: The authors declare no conflict of interest.

References

1. Tang, B.; Sun, Y.; Wu, S.; Gao, K.; Yan, X.; Zeng, F. Comprehensive Evaluation and Application of GIS Insulation Condition Part 2: Construction and Application of Comprehensive Evaluation Model Considering Universality and Economic Value. *IEEE Access* **2019**, *7*, 129127–129135. [CrossRef]
2. Nitta, T.; Shibuya, Y.; Fujiwara, Y.; Arahata, Y.; Takahashi, H.; Kuwahara, H. Factors Controlling Surface Flashover in SF6 Gas Insulated Systems. *IEEE Trans. Power Appar. Syst.* **1978**, *3*, 959–968. [CrossRef]
3. Abdollah, M.; Razi-Kazemi, A.A. Intelligent Failure Diagnosis for Gas Circuit Breakers Based on Dynamic Resistance Measurements. *IEEE Trans. Instrum. Meas.* **2018**, *68*, 3066–3077. [CrossRef]
4. Zhou, W.; Zheng, Y.; Yang, S.; Li, H.; Wang, B.; Qiao, S. Detection of intense partial discharge of epoxy insulation in sf6 insulated equipment using carbonyl sulfide. *IEEE Trans. Dielectr. Electr. Insul.* **2016**, *23*, 2942–2948. [CrossRef]
5. Cai, W.; Tang, J.; Cheng, L.; Zhang, C.; Fan, M.; Zhou, Q.; Yao, Q. Detection of SF6 Decomposition Components Under Partial Discharge by Photoacoustic Spectrometry and its Temperature Characteristic. *IEEE Trans. Instrum. Meas.* **2016**, *65*, 1343–1351. [CrossRef]
6. Braun, J.M.; Chu, F.Y.; Seethapathy, R. Characterization of GIS Spacers Exposed to SF6 Decomposition Products. *IEEE Trans. Electr. Insul.* **1987**, *22*, 187–193. [CrossRef]
7. Chu, F.Y. SF6 Decomposition in Gas-Insulated Equipment. *IEEE Trans. Electr. Insul.* **1986**, *EI-21*, 693–725. [CrossRef]
8. Han, D.; Lin, T.; Zhang, G.; Liu, Y.; Yu, Q. SF6 gas decomposition analysis under point-to-plane 50 Hz AC corona discharge. *IEEE Trans. Dielectr. Electr. Insul.* **2015**, *22*, 799–805. [CrossRef]
9. Yang, D.; Tang, J.; Zeng, F.; Yang, X.; Yao, Q.; Miao, Y.; Chen, L. Correlation characteristics between SF6 decomposition process and partial discharge quantity under negative DC condition initiated by free metal particle defect. *IEEE Trans. Dielectr. Electr. Insul.* **2018**, *25*, 574–583. [CrossRef]
10. Wang, J.; Ding, W.; Yan, J.; Wang, Y.; Wang, Y.; Li, Z.; Li, G. Decomposition characteristics of SF6 under overheating conditions. *IEEE Trans. Dielectr. Electr. Insul.* **2017**, *24*, 3405–3415. [CrossRef]
11. Zeng, F.; Lei, Z.; Yang, X.; Tang, J.; Yao, Q.; Miao, Y. Evaluating DC Partial Discharge with SF 6 Decomposition Characteristics. *IEEE Trans. Power Deliv.* **2019**, *34*, 1383–1392. [CrossRef]
12. Zhang, X.; Xiao, S.; Zhang, J.; Li, C.; Dai, Q.; Han, Y. Influence of humidity on the decomposition products and insulating characteristics of CF3I. *IEEE Trans. Dielectr. Electr. Insul.* **2016**, *23*, 819–828. [CrossRef]
13. Zhang, X.; Tian, S.; Xiao, S.; Huang, Y.; Liu, F. Partial discharge decomposition characteristics of typical defects in the gas chamber of SF6 insulated ring network cabinet. *IEEE Trans. Dielectr. Electr. Insul.* **2017**, *24*, 1794–1801. [CrossRef]
14. Tang, J.; Liu, F.; Zhang, X.; Meng, Q.; Zhou, J. Partial discharge recognition through an analysis of SF6 decomposition products part 1: Decomposition characteristics of SF6 under four different partial discharges. *IEEE Trans. Dielectr. Electr. Insul.* **2012**, *19*, 29–36. [CrossRef]
15. Tang, J.; Liu, F.; Meng, Q.; Zhang, X.; Tao, J. Partial discharge recognition through an analysis of SF6 decomposition products part 2: Feature extraction and decision tree-based pattern recognition. *IEEE Trans. Dielectr. Electr. Insul.* **2012**, *19*, 37–44. [CrossRef]
16. Pang, X.; Zhen, L.; Long, Y.; Yu, K.; Xiu, S. Study on Gas Decomposition Characteristics of SF 6 with Moisture After Current Interruption. In Proceedings of the 2019 5th International Conference on Electric Power Equipment—Switching Technology (ICEPE-ST), Kitakyushu, Japan, 13–16 October 2019.
17. Zeng, F.; Tang, J.; Zhang, X.; Sun, H.; Yao, Q.; Miao, Y. Study on the Influence Mechanism of Trace H2O on SF6 Thermal Decomposition Characteristic Components. *IEEE Trans. Dielectr. Electr. Insul.* **2015**, *22*, 766–774. [CrossRef]
18. Yan XWang, C.; Ji, Y.; Guo, Y. Application of Decomposition Products Detection of SF6 in Switchgears. *Power Syst. Technol.* **2010**, *34*, 160–165.
19. Yan, X.L.; Wang, C.Y.; Song, G.; Ji, Y.S.; Yang, R.; Zhang, X. Recent Progress in Detection of SF6 Decomposition Products and Fault Diagnosis for Gas Insulated Switchgears. *High Volt. Appar.* **2013**, *49*, 1–10.
20. Sauers, I.; Ellis, H.W.; Christophorou, L.G. Neutral Decomposition Products in Spark Breakdown of SF6. *IEEE Trans. Electr. Insul.* **1986**, *EI-21*, 111–120. [CrossRef]

21. Lee, S.J.; Theerthagiri, J.; Nithyadharseni, P.; Arunachalam, P.; Balaji, D.; Kumar, A.M.; Madhavan, J.; Mittal, V.; Choi, M.Y. Heteroatom-doped graphene-based materials for sustainable energy applications: A review. *Renew. Sustain. Energy Rev.* **2021**, *143*, 110849. [CrossRef]
22. Theerthagiri, J.; Karuppasamy, K.; Lee, S.J.; Shwetharani, R.; Kim, H.S.; Pasha, S.K.; Ashokkumar, M.; Choi, M.Y. Fundamentals and comprehensive insights on pulsed laser synthesis of advanced materials for diverse photo-and electrocatalytic applications. *Light Sci. Appl.* **2022**, *11*, 1–47. [CrossRef] [PubMed]
23. Catauro, M.; Tranquillo, E.; Poggetto, G.D.; Naviglio, S.; Barrino, F. Antibacterial Properties of Sol–Gel Biomaterials with Different Percentages of PEG or PCL. *Macromol. Symp.* **2020**, *389*, 1900056. [CrossRef]
24. Qi, B.; Li, C.R.; Luo, L.S.; Zhang, Y.; Zheng, S.S. Experiment on the Correlation Between Partial Discharge and Gas Decomposition Products in GIS. *High Volt. Eng.* **2010**, *36*, 957–963.
25. Yang, R.; Xu, M.; Yan, J.; Yang, M.; Geng, Y.; Liu, Z.; Wang, J. Decomposition Characteristics of SF6 under Arc Discharge and the Effects of Trace H2O, O2, and PTFE Vapour on Its By-Products. *Energies* **2021**, *14*, 414. [CrossRef]
26. Fu, L.; Guan, Y.; Zhang, L.; Zhang, D.; Wang, H.; Chi, J.; Wei, B. A potential fault of circuit breaker found using SF6 decomposition products detection. *J. Phys. Conf. Ser.* **2022**, *2246*, 012004. [CrossRef]
27. Cheng, P.; Shayesteh, A.; Bohme, D.K. Gas-phase reactions of sulfur hexafluoride with transition metal and main group atomic cations: Room-temperature kinetics and periodicities in reactivity. *Inorg. Chem.* **2009**, *48*, 1018–1029. [CrossRef]
28. Miyagi, K.; Kagami, K.; Sugimoto, T. Breakdown Effects of Dissolved SF6 Gas on Uniform Field in Perfluorocarbon Liquid. *IEEJ Trans. Fundam. Mater.* **1999**, *119*, 311–316. [CrossRef]
29. Zebouchi, N.; Li, H.; Haddad, M.A. Development of Future Compact and Eco-Friendly HVDC Gas-Insulated Systems: Shape Optimization of a DC Spacer Model and Novel Materials Investigation. *Energies* **2020**, *13*, 3288. [CrossRef]
30. Liu, H.; Deng, K.; Fu, H.J.; Ma, W.J. Investigation on the Relationship Between SF_6 Gas Decomposition and GIS Equipment Operating Status. *Gaoya Dianqi/High Volt. Appar.* **2013**, *49*, 127–132.
31. Lijun, F.; Guan, Y.; Zhang, L.; Jin, H.; Wang, H.; Jing, Y. Study on the mechanism and influencing factors of SF6 decomposition products. *IOP Conf. Ser. Earth Environ. Sci.* **2021**, *657*, 012039. [CrossRef]
32. Zhang, X.; Tie, J.; Chen, Q.; Xiao, P.; Zhou, M. Pt-doped TiO2-based sensors for detecting SF6 decomposition components. *IEEE Trans. Electr. Insul.* **2015**, *22*, 1559–1566.
33. Zeng, F.; Luo, J.; Tang, J.; Zhou, Q.; Yao, Q. Stainless Steel; Studies in the Area of Stainless Steel Reported from Wuhan University (Influence Regularity of Aluminum, Copper and Stainless-steel on SF6 PD Decomposition Characteristics Components). *Chem. Chem.* **2017**, *26*, 1470–1476.
34. Wang, J. *Vacuum Arcing Chamber Design, Manufacture and Application*; Xi'an Jiaotong University Press: Xi'an, China, 1993; pp. 50–56.
35. Naef, O.; Zimmerman, C.P.; Beehler, J.E. Proposed Transient Recovery Voltage Ratings for Power Circuit Breakers. *IEEE Trans. Power Appar. Syst.* **1965**, *84*, 580–608. [CrossRef]
36. Wu, Q.; Wang, Y.; Wang, Y.; Wang, J.; Lan, L.; Deng, Y.; Wen, X.; Luo, B.; Xiao, W. Ablation state assessment of SF6 circuit breaker contacts based on BP neural network and mean impact value. *Energy Rep.* **2022**, *8*, 874–883. [CrossRef]
37. Zhu, Y.; Yang, J.; Shen, J. Analysis and research on contact ablation of high voltage circuit breake. *Power Equip.* **2022**, *35*, 5.
38. Cojocaru-Mirédin, O.; Schmieg, J.; Müller, M.; Weber, A.; Ivers-Tiffée, E.; Gerthsen, D. Quantifying Lithium in Lithium-ion battery solid electrolyte by atom probe tomography correlated with high-resolution scanning electron microscopy. *Microsc. Microanal.* **2022**, *28* (Suppl. S1), 760–762. [CrossRef]